J. Fluid Mech. (2025), *vol.* 1009, R2, doi:10.1017/jfm.2025.299



Transient characteristics of fully localised turbulence in transitional channel flow

Yuze Wu[1] **and Baofang Song**[1]

[1]State Key Laboratory for Turbulence and Complex Systems and HEDPS, Center for Applied Physics and Technology, College of Engineering, Peking University, Beijing 100871, PR China

Corresponding author: Baofang Song, baofang.song@pku.edu.cn

(Received 26 December 2024; revised 19 February 2025; accepted 14 March 2025)

The temporal characteristics of fully localised turbulent bands in transitional channel flow remains unclear due to the difficulty in resolving the large length and time scales involved. Here, we tackle this problem by performing statistical lifetime studies in sufficiently large computational domains. The results show signs of stochastic memoryless decay of a fully localised band, suggesting a chaotic-saddle behaviour of the entire band as a coherent entity. Although the mean lifetime of a turbulent band was reported to increase with the band length, our data suggest that it saturates at a certain length. This saturation results in a characteristic lifetime for a fully developed band with a changing length due to the intermittent chipping and decay of turbulence at the upstream end. This memoryless behaviour is observed down to Reynolds number $Re = 630$ in our study and we propose that the onset of the memoryless behaviour is in the range of $Re \simeq 620{-}630$. Our data also show that the time it takes for a perturbed flow to enter the saddle, i.e. to start behaving memorylessly, can be thousands of convective time units, which is comparable to the maximum achievable observation time in existing channel set-ups and may pose difficulties for experiments.

Key words: transition to turbulence, turbulent transition

1. Introduction

Localised turbulence in subcritical transition of pipe and Couette flows has been shown to be transient in nature, i.e. the turbulence will decay at a finite time with a characteristic mean lifetime at a given Reynolds number, Re, and the decay was shown to be stochastic and memoryless (Hof *et al.* 2006; Peixinho & Mullin 2006; Willis & Kerswell 2007; Avila *et al.* 2010; Borrero-Echeverry *et al.* 2010; Shi *et al.* 2013). This memoryless transient nature is essential for the analogy between transition to turbulence and directed percolation phase transition (DP) (Hinrichsen 2000; Barkley 2016; Lemoult *et al.* 2016; Shih *et al.*

© The Author(s), 2025. Published by Cambridge University Press.

https://doi.org/10.1017/jfm.2025.299 Published online by Cambridge University Press

2016; Chantry *et al.* 2017; Hof 2022; Klotz *et al.* 2022; Lemoult *et al.* 2024), and has been expected to be universal to localised turbulence in all basic shear flows. However, the temporal characteristics of localised turbulence in channel flow remain unclear and debated to date.

At transitional Reynolds numbers, localised turbulence in channel flow can organise itself into a banded structure obliquely oriented about the streamwise direction (Tsukahara *et al.* 2005; Tuckerman *et al.* 2014). If the turbulent band is strongly constrained by a narrow periodic dimension along the band (see figure 1*b*), effectively resulting in an infinite periodic band (referred to as the quasi-one-dimensional band hereafter), similar memoryless decay was found (Gomé *et al.* 2020, 2022). However, in a sufficiently large flow domain, a turbulent band becomes fully localised (i.e. with a finite length) by forming an upstream end and a downstream end (Xiong *et al.* 2015; Kanazawa 2018; Tao *et al.* 2018; Paranjape 2019; Shimizu & Manneville 2019; Kashyap *et al.* 2020; Song & Xiao 2020; Xiao & Song 2020*a*, *b*; Mukund *et al.* 2021; Marensi *et al.* 2023), see figure 1(*a*) for a sketch. The dynamics at the two ends are asymmetric with turbulence being generated continuously at the downstream end (referred to as *head* hereafter) and decaying or chipping intermittently at the upstream end (referred to as *tail* hereafter). The generation of turbulence at the head is through nearly periodic streak and vortex generation (Kanazawa 2018; Paranjape 2019; Xiao & Song 2020*a*; Mukund *et al.* 2021; Marensi *et al.* 2023), which was attributed to either an inflectional crossflow instability associated with the local meanflow (Song & Xiao 2020; Xiao & Song 2020*a*, *b*) or a localised exact coherent structure (Kanazawa 2018). This dynamics at the head was shown to be essential for the growth and self-sustaining mechanism of the whole band (Song & Xiao 2020; Mukund *et al.* 2021; Wu & Song 2022; Marensi *et al.* 2023) and contributes to the tilt angle selection for the band as well (Zhang & Tao 2023).

After being seeded, a short band will grow in length l initially due to the faster turbulence generation at the head. However, the chipping and decay of turbulence at the tail eventually will limit l and keep it finite, which is $O(100)$ channel heights at $Re \simeq 660$ and increases with Re (Kanazawa 2018). In this paper, Re is based on the half-channel height h (will be used as the length unit hereafter), the centreline velocity of the basic laminar flow and the fluid viscosity. Besides the length scale, the time scale of a turbulent band is also large. Above $Re \simeq 660$, it can evolve for approximately 10^4 time units without a sign of decay (Kanazawa 2018; Tao *et al.* 2018; Paranjape 2019; Xiao & Song 2020*a*). These two factors require large flow domain and observation time for clarifying the temporal behaviour of a band in either experiments or direct numerical simulations (DNS).

Some studies, from different perspectives, proposed that a turbulent band becomes sustained above a critical Re. Kanazawa (2018) proposed $Re \simeq 660$ because the exact coherent structure they identified at the head appears at $Re \simeq 660$ and is stable. Tao *et al.* (2018) proposed that a band can become sustained at $Re \simeq 700$ via breaking and reconnecting in a computation box with a specific aspect ratio, based on an observation time of 10^4. Paranjape (2019) proposed $Re \simeq 650$ because band growth outweighs shrinking on average at higher Re whereas it is the opposite otherwise. The observation time in their experiment was $O(10^3)$, which is the largest reported for experiments to our knowledge. Shimizu & Manneville (2019) proposed $Re \approx 700$ by DNS based on an observation time of 1.5×10^5, but the conclusion was drawn for the global turbulent state in a large periodic flow domain rather than for a single turbulent band. In comparison, in the quasi-one-dimensional case, the band is of a lifetime of just $O(10^2)$ at $Re \simeq 700$ and remains transient up to $Re \simeq 1000$ (Gomé *et al.* 2020), indicating that the full localisation makes a significant difference. If a band indeed becomes sustained at a critical Re, it would lead to a completely different transition route to turbulence compared with pipe and Couette flows.

https://doi.org/10.1017/jfm.2025.299 Published online by Cambridge University Press

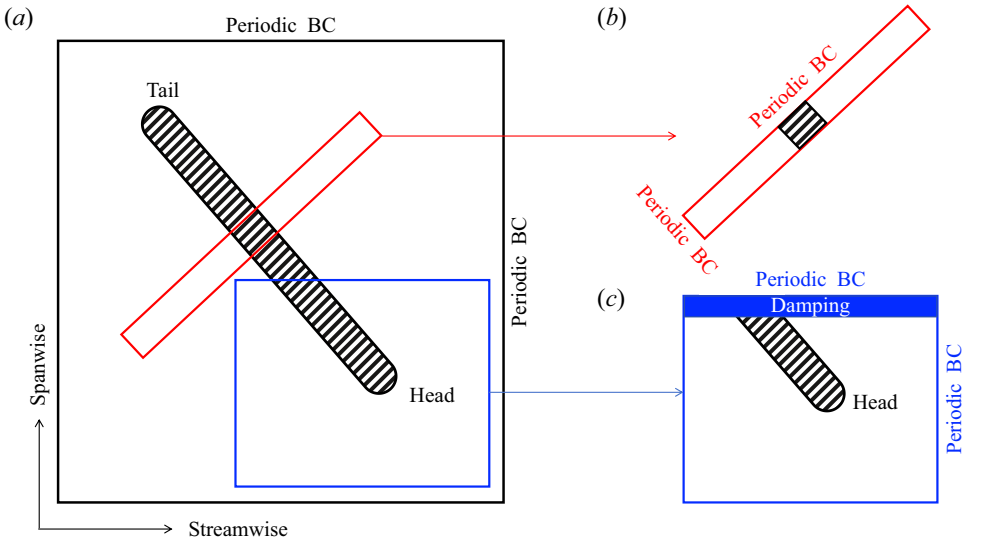


Figure 1. Sketches of the flow domains for studying turbulent band in channel flow in numerical simulations. The shaded area represents turbulent region and blank area represents laminar region. (*a*) The normal computational box with one edge parallel to the streamwise direction. (*b*) The tilted narrow computational box with the short edge parallel to the band. (*c*) The normal box with a small damping region, both of which co-move with the head of the band. Periodic boundary conditions (BCs) are imposed as indicated in the figure.

Due to the large length and time scales of fully developed bands, statistical investigation was lacking in previous DNS studies where conclusions were made based on a single or only a few realisations, while it was difficult to achieve long observation times in experiments. To manage a statistical study with sufficiently long observation times, Xu & Song (2022) considered a moderately constrained band by keeping the head while damping the tail (see figure 1*c*). This technique allows the authors to fix and control l so as to prepare well-controlled initial conditions and reduce costs. In the parameter regime of $l \leqslant 70$ and $Re \leqslant 675$, the authors observed memoryless decay and the length-dependent nature of the mean lifetime. The lifetime increases quickly with both increasing l and Re but remains finite in this parameter regime. For example, the mean lifetime is already larger than 10^4 for $Re = 655$ with $l \approx 70$ and $Re = 665$ with $l \approx 54$. Decay was also observed in a single run at $Re = 685$ with $l \approx 38$ (survival time $O(10^5)$) and $Re = 660$ with $l \approx 110$ (survival time $O(10^4)$), but statistical studies were not carried out because of the large lifetime. The authors conjectured that a fully developed band is transient by nature and the discrepancies between the reported critical Re values for sustained turbulence are possibly attributed to the different observation times and lack of statistics. However, the band lengths considered in Xu & Song (2022) were much shorter than the fully developed ones and were artificially fixed, i.e. the artificial constraint was still rather strong; it is unclear whether a fully developed band with a naturally varying length, due to the intermittent chipping and decay of the turbulence at the tail, is still transient and memoryless. The aim of this paper is to clarify this problem by considering fully developed bands.

2. Methods

The same numerical method as described in Xu & Song (2022) is used here. Given the low Re, 56 Chebyshev grid points and a finite-difference differentiation with a 9-point stencil are used in the wall-normal direction (y). Periodic BCs and Fourier spectral methods are

https://doi.org/10.1017/jfm.2025.299 Published online by Cambridge University Press

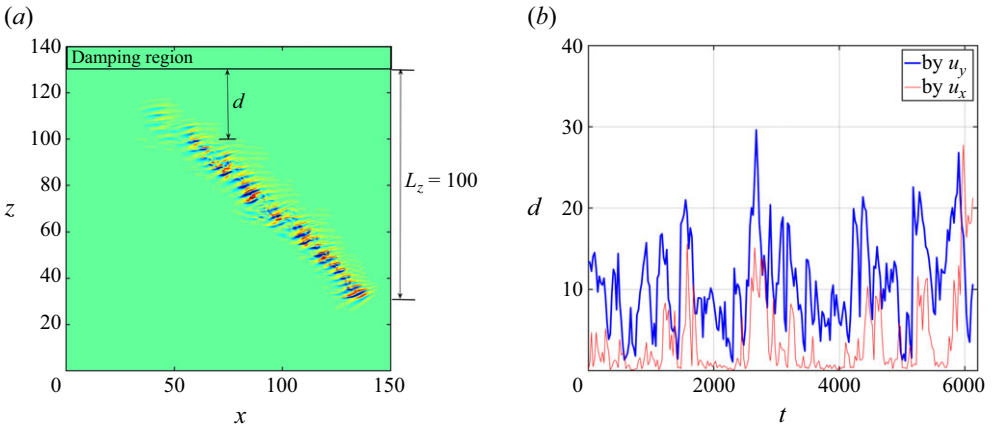


Figure 2. The computational box (*a*) and the distance between the damping region and the tail of a turbulent band (*b*). In (*a*), wall-normal velocity fluctuation u_y is plotted in the $x-z$ cutplane at $y=-0.5$. Red colour represents positive and blue represents negative values. The head of the band is fixed at $z=30$ and the damping region is between $z=130$ and 140. The spanwise distance between the tail and the damping region is denoted as d. Panel (*b*) shows the time series of the distance d for a run at $Re=640$. The blue curve is based on u_y and the red curve is based on u_x. Panel (*a*) is taken at $t=2500$ from the time series shown in (*b*).

used in the streamwise (x) and spanwise (z) directions, and the grid sizes are $h/\Delta x=4.6$ and $h/\Delta z=5.5$ in these two directions, respectively. This resolution is comparable to those used in the literature for studying turbulent band at slightly higher Reynolds numbers (Kanazawa 2018; Tao *et al.* 2018; Shimizu & Manneville 2019; Kashyap *et al.* 2020; Marensi *et al.* 2023). The time-step size is fixed at $\Delta t=0.025$. This setting assures a decrease of nearly four orders of magnitude in the spectra of the maximum amplitude of the Fourier coefficient of the velocities in the whole domain. A constant mass flux is imposed by dynamically adjusting the driving pressure gradient. More details about the numerical method can be found in Xiao & Song (2020*a*) and Xu & Song (2022).

Following Xu & Song (2022), a computation setting as sketched in figure 1(*c*) is used in this study. The computation box moves, keeping the head of the band fixed at approximately $z=30$. An average speed of the head was measured every 25 time units and then the speed of the computation box was adjusted accordingly. The streamwise and spanwise sizes are $l_x=150$ and $l_z=140$, respectively, the damping region is $130<z<140$ and the head is located at $z=30$, see figure 2(*a*). Therefore, the distance between the head and the damping region is $L_z=100$, which sets the maximum of the spanwise length of a band. Correspondingly, the maximum band length is $l\approx 160$ given that the tilt angle of a band about the streamwise direction is approximately 40° in the Re regime considered here (Tao *et al.* 2018; Paranjape 2019; Xiao & Song 2020*b*; Zhang & Tao 2023). Reynolds numbers 640 and 630 are chosen for this study.

Figure 2(*b*) shows the spanwise distance d between the tail of a rather long-lived band and the damping region at $Re=640$. It can be seen that d is considerably larger than zero in a large portion of the time, especially when d is measured using the wall-normal velocity fluctuation u_y. This indicates that, often, the tail of this band does not reach the damping region, i.e. the computation setting shown in figure 2(*a*) allows to account for the factor of length variation. The velocity streaks at the tail can reach the damping region more often; see the time windows in which $d\approx 0$ based on the streamwise velocity fluctuation u_x in figure 2(*b*). Therefore, the damping region is necessary for damping out these streaks, or a segment of band chipped off so that the head will not be affected by them due to the

https://doi.org/10.1017/jfm.2025.299 Published online by Cambridge University Press

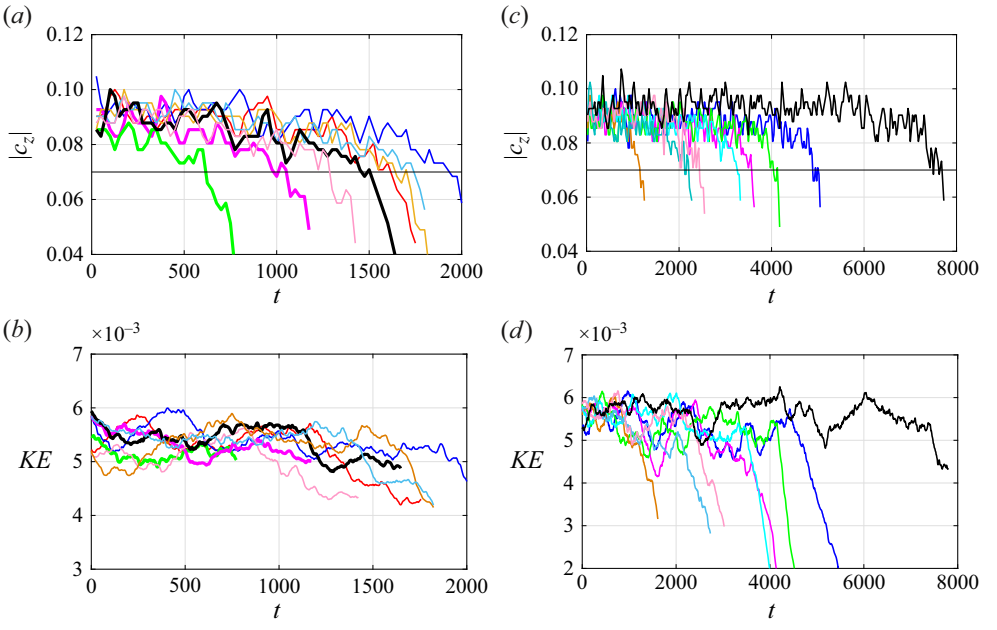


Figure 3. The spanwise speed of the head $|c_z|$ (*a, c*) and the kinetic energy of turbulent velocity fluctuations KE (*b, d*) of a few runs at $Re = 630$ (*a, b*) and 640 (*c, d*). The same computation setting as shown in figure 2(*a*) is used. The horizontal straight line in (*a, c*) denotes $c_z = 0.07$ which can be used as the threshold for determining a decay event.

periodic BC. It should be noted that, in a larger domain without the damping, a band may temporarily get considerably longer than the limit set by our setting (see supplementary movie 1 available at https://doi.org/10.1017/jfm.2025.299). Nevertheless, we will show more quantitatively later in § 3 that this setting allows the band to fully develop in terms of the mean lifetime.

We use the Reynolds-number-quenching technique to perturb the flow. Specifically, velocity snapshots from long-lived turbulent bands simulated in the same computation setting at $Re = 645$, 650 and 660 are used as the initial conditions. This assures that all initial conditions are highly similar. The head has nearly constant streamwise and spanwise travelling speeds during the lifetime of a band, but will slow down when the band starts to decay (Paranjape 2019; Mukund *et al.* 2021; Xu & Song 2022); see Appendix A for more details about the decay process. Therefore, spanwise speed of the head $|c_z|$ is a candidate for the diagnosis of a decay event, see figure 3(*a, c*). Note that this speed can be negative or positive depending on the orientation of the band. The orientation we chose actually gives a negative speed, i.e. the head moves to the negative z direction. However, we will refer to $|c_z|$ as the spanwise speed in the following. The traditional diagnosis, the total kinetic energy of the turbulent fluctuations (KE), does not serve as well as $|c_z|$ at $Re = 630$ when the lifetime is short (see figure 3*b*). Firstly, the decrease of KE is less sharp. Secondly, the decrease of $|c_z|$ and KE are often not synchronised, i.e. KE may have not started decreasing when $|c_z|$ has already decreased significantly; see the bold green, magenta and black curves in figure 3(*a, b*). If the decay is to be diagnosed by setting a sufficiently low threshold in KE, this time delay could significantly affect the measured lifetime when the lifetime itself is short. Thirdly, a longer decaying band may even have larger kinetic energy than a shorter sustaining band. Therefore, $|c_z|$ is chosen as the diagnosis of the decay of

https://doi.org/10.1017/jfm.2025.299 Published online by Cambridge University Press

a band. Nevertheless, KE may work equally well for $Re = 640$ at which the lifetime is much larger than the above-mentioned time delay (see figure 3*d*).

Figure 3 indicates a stochastic behaviour of the decay and sensitive dependence on the initial conditions. Following the method of Avila *et al.* (2010), for a stochastic decay process, the survival rate is defined as $S(t) = P\{\text{survival time} \geqslant t\}$ and the escape rate can be defined as $\kappa = -1/S(t)\mathrm{d}S(t)/\mathrm{d}t$. For a process that only becomes memoryless after a time instance t_0, there would be $\kappa = \text{const.}$ and consequently $S(t) \propto \exp(-\kappa(t - t_0))$ for $t > t_0$. Then $S(t)$ would correspond to the distribution function of an exponential distribution, and the mean (mathematical expectation) lifetime of the process is given by $\tau = 1/\kappa$. In a random experiment, τ can be estimated with the sample mean of the decay time if the population obeys an exponential distribution. The estimation of κ will simply be taken as the inverse of the estimated τ.

However, t_0 is not known *a priori*. In practice, selecting a value arbitrarily, the subsample in which the turbulence survives longer than t_0 will be used for the estimation. Then, t_0 is gradually increased and the same procedure is repeated. A t_0-independent estimation of τ (also κ) is supposed to be obtained if the entire subsample has started obeying an exponential distribution. In this case, it is considered that the decay has become memoryless and the turbulent trajectory has entered a chaotic saddle (Faisst & Eckhardt 2004; Schneider & Eckhardt 2008; Avila *et al.* 2010). In the following, we show the statistics where the estimations are still denoted as τ and κ.

3. Results

Statistics for $Re = 640$ are shown in figure 4. It requires setting a proper threshold in $|c_z|$ below which the turbulent trajectory is considered to have escaped from the saddle. As the speed $|c_z|$ mainly fluctuates between 0.08 and 0.1 during the lifetime (figure 3*c*), $c_z = 0.065$ is used as the threshold for detecting a decay event. Because the survival time is several thousand and the drop in $|c_z|$ is sharp during the decay on this time scale, as shown in figure 3(*c*), different thresholds, say 0.07 and 0.06, do not make a significant difference in our tests.

The damping with $L_z = 100$ still constrains the band and could still affect the lifetime. Due to the chaotic nature of turbulence, it certainly will affect the lifetime of an individual band, but here we show the saturation of the mean lifetime with respect to L_z. Beside $L_z = 100$, two lower values of $L_z = 80$ and 60 are considered to realise two smaller band lengths (recall the definition of L_z in figure 2*a*). Figure 4(*a*) shows the survival rate for the three cases. For the shortest case $L_z = 60$, corresponding to the band length of $l \approx 93$, the slope of the tail of S is significantly larger than the other two cases, indicating a shorter lifetime, in agreement with the size-dependence of the lifetime reported by Xu & Song (2022). It is difficult to conclude whether or not there is a plateau region in κ with the sample considered. A plateau might be forming after $t \approx 1800$ but the data points are rather scattered (see figure 4*b*). Nevertheless, straightness can be observed in the tail of the $S{-}t$ plot as shown in figure 4(*a*) and the inset. Using $t_0 = 1825$, which gives a subsample size of $N_s = 58$, we get $\tau = 436 \pm 112$ with 95 % confidence ($\pm 1.96/\sqrt{N_s}$ times the sample mean). The exponentials $ae^{-\kappa(t-t_0)}$ with these estimations, where $a = S(t_0)$, seem to fit the tail of S reasonably well (see figure 4*a* and the inset). On the other hand, the slopes of the tails of the other two cases seem to be parallel straight lines in the semilog-scale plot, suggesting exponentially distributed lifetimes and equal mean lifetimes. These can be more quantitatively shown in terms of the escape rate κ. As figure 4(*b*) shows, the estimated κ increases initially with increasing t_0 but seems to approach a plateau when t_0 is sufficiently large. Note that the plateau starts at $t_0 \approx 2300$ for the case of $L_z = 80$ and at $t_0 \approx 3500$ for

https://doi.org/10.1017/jfm.2025.299 Published online by Cambridge University Press

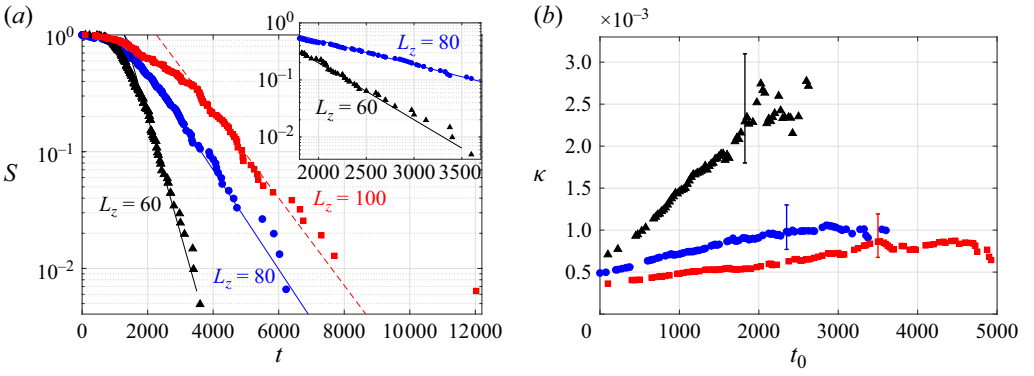


Figure 4. The survival rate S as a function of time t (a) and the escape rate κ as a function of t_0 (b) for $Re = 640$. Three values of L_z are considered, namely, $L_z = 100$ (red squares), 80 (blue circles) and 60 (black triangles) to check the variation of τ with the band length. The sample sizes are 152, 151 and 203, respectively. In (a), the black line is $0.296e^{-\kappa(t-t_0)}$ with $t_0 = 1825$ and $\kappa = 0.00292$, the blue solid line is $0.351e^{-\kappa(t-t_0)}$ with $t_0 = 2350$ and $\kappa = 0.00098$, and the red dashed line is $0.345e^{-\kappa(t-t_0)}$ with $t_0 = 3500$ and $\kappa = 0.00086$. The inset shows a zoom-in view of the $L_z = 60$ and 80 cases.

the case of $L_z = 100$, indicating large initial transient times for the flow to enter a chaotic saddle from the initial conditions quenched from higher Re. For the $L_z = 80$ case, using $t_0 = 2350$, we get $\tau = 1020 \pm 277$ with $N_s = 52$. For $L_z = 100$, the same estimation at $t_0 = 3500$ gives $\tau = 1160 \pm 322$ with $N_s = 50$. The corresponding exponentials fit the tail of S well (see the lines in figure 4a). The errorbars in figure 4(b) correspond to these confidence intervals, which overlap to a large extent. The two estimated lifetimes are close and cannot be separated given the current statistical uncertainty, suggesting that the mean lifetimes of a band in these two settings are approximately equal. In fact, if the exceptionally long-lived run in the $L_z = 100$ case (decay time is 12 000, see the point on the far right in figure 4a which deviates largely from the exponential) was removed, the two lifetimes would be much closer. Both of them are significantly larger than the lifetime of the $L_z = 60$ case within the statistical uncertainties. Besides, the results indicate that the damping setting L_z may influence t_0 considerably, and the less constrained the turbulence, the larger the t_0.

This observation suggests that, although the mean lifetime was shown to increase with the band length in the relatively short-length regime (Xu & Song 2022), the lifetime would saturate at a certain length (at least there is a clear trend of a saturation) such that the variation occurring at the tail of a band does not affect its mean lifetime anymore. The distance $L_z = 100$ seems sufficiently large for the lifetime study at $Re = 640$, which should be large enough for lower Reynolds numbers and is used for the study at $Re = 630$ also.

At $Re = 630$, since the survival times of turbulent bands are much shorter than those at $Re = 640$, the threshold in c_z used to detect a decay event may matter. Given that $|c_z|$ mostly fluctuates between 0.08 and 0.1 in the lifetime of a band (see figure 3a), the values 0.07, 0.065 and 0.06 are considered and the results are compared in figure 5(a). For each threshold, there seems to be an exponential tail after $t \simeq 1000$, which is further evidenced by the appearance of a plateau in the κ–t_0 plot at $t_0 > 1000$. The slopes of the tails of S seem to be close to each other, and the plateaus of κ also seem to overlap roughly. Although there are rather strong scattering of the data in the plateau region, all data fall in the 95 % confidence interval of the κ estimated at $t_0 = 1025$ for the $|c_z| = 0.065$ case (see the error bar in figure 5b). This observation is expected for exponentially distributed lifetime because the lifetime difference caused by different thresholds can be absorbed in t_0; consequently, the estimated mean lifetime should not be affected by the specific

https://doi.org/10.1017/jfm.2025.299 Published online by Cambridge University Press

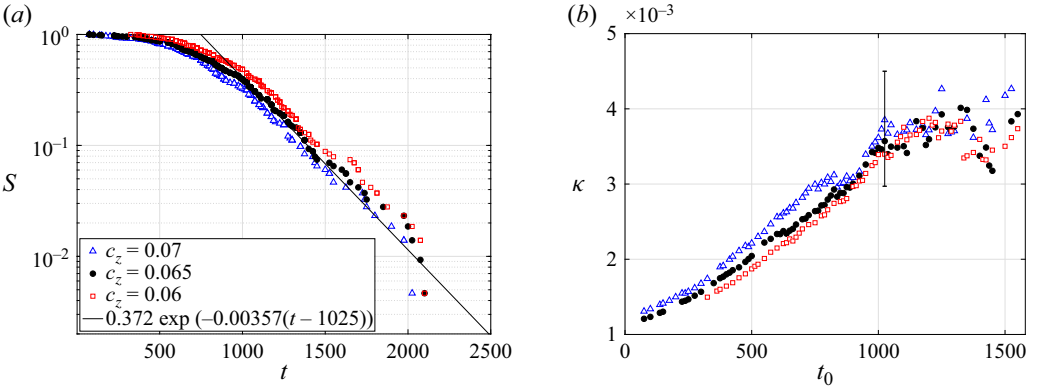


Figure 5. The survival rate S as a function of time t (a) and the escape rate κ as a function of t_0 (b) at $Re = 630$. The sample size is 215. Three thresholds in c_z for detecting the decay are considered, which are 0.07 (blue triangles), 0.065 (black circles) and 0.06 (red squares). The solid line in (a) is $0.372e^{-\kappa(t-t_0)}$ with $t_0 = 1025$ and $\kappa = 0.00357$, taken from the data shown as black circles in (b).

threshold. Therefore, the time after which the decay becomes memoryless can be estimated to be $t_0 \approx 1000$ and the corresponding $\kappa \approx 0.0035$. The exponential with $t_0 = 1025$ and $\kappa = 0.00357$ (the black line in figure 5a), which are taken from the estimation using the threshold $c_z = 0.065$, seems to fit the corresponding S data (black squares) well and parallel to the tails of the other two data sets also. Correspondingly, with the subsample size $N_s = 78$, the estimated mean lifetime is $\tau \approx 280 \pm 62$ with 95 % confidence.

We want to mention that the large scattering in κ for the $(Re, L_z) = (640, 60)$ and $Re = 630$ cases may not be solely attributed to the sample size because the sample sizes of the $(Re, L_z) = (640, 80)$ and $(Re, L_z) = (640, 100)$ cases are even smaller, whereas their κ shows smaller scattering. The large scattering is possibly caused by the relatively short time span of the subsample, i.e. short $t - t_0$, and the relatively low temporal resolution of the lifetime values. Note that in our simulations, head speed was measured every 25 time units so that the temporal resolution of the lifetime is at best 25. It will not be a problem if the time span of the subsample is large because the resolution of the lifetime is small compared with this time span, but may cause large data scattering otherwise. A speed measurement method that can better resolve the lifetime may help ease this problem.

4. Discussion and conclusion

Unlike for turbulent puffs in pipe flow, discrepancies between views on the temporal characteristics of a fully localised turbulent band in channel flow remain to date (Kanazawa 2018; Tao *et al.* 2018; Paranjape 2019; Shimizu & Manneville 2019; Mukund *et al.* 2021; Xu & Song 2022). Through extensive computer simulations, our results, for the first time to our knowledge, showed signs for the memoryless transient characteristic of a localised band as a coherent entity, demonstrating a similarity between a turbulent band and a turbulent puff.

We investigated low Reynolds numbers down to $Re = 630$, at which $\tau \approx 280$. This memoryless behaviour likely persists to lower Re; however, as Re decreases further, it is increasingly difficult to distinguish a trajectory that visits the saddle for a short time from one that simply reverts to the laminar state without entering the saddle. Given the sharp change of τ with respect to Re, as shown by Xu & Song (2022) and indicated by the comparison between the τ values for $Re = 640$ and 630 here, the onset of memoryless

https://doi.org/10.1017/jfm.2025.299 Published online by Cambridge University Press

decay should be close to $Re = 630$. In fact, Mukund *et al.* (2021) observed an ageing behaviour of the decay at $Re = 618$ in experiments. Therefore, we propose that the onset of this memoryless behaviour is in the range of $Re \simeq 620 - 630$.

Although Xu & Song (2022) showed that the mean lifetime increases quickly with the band length in the relatively short-length regime, here, the result for $Re = 640$ suggests that there exists a critical length above which the lifetime does not change anymore. In other words, a band starts to exhibit a characteristic mean lifetime only when it has sufficiently developed. However, at $Re > 640$, the lifetime will be much larger and the computation cost will be too high for a statistical study to determine this critical length and the corresponding saturated mean lifetime. It seems also challenging for experiments due to the large t_0, which, depending on the details of the initial conditions, can be several thousand convective time units and comparable to the maximum achievable observation time in existing channel set-ups (Paranjape 2019; Mukund *et al.* 2021). In contrast, t_0 for turbulent puffs in pipe flow is only approximately one hundred convective time units (Hof *et al.* 2008; Schneider & Eckhardt 2008; Avila *et al.* 2010), much smaller than the achievable observation time in usual pipe set-ups. Thus, the mean lifetime can be measured by sufficiently many realisations even though it is also large, thanks to the memorylessness (Hof *et al.* 2006, 2008; Avila *et al.* 2010). The difference in t_0 in these two flows is probably attributed to the different constraints of the flow by the solid wall: the stronger the constraint, the faster the flow adjusts after quenching so that the smaller the t_0. Currently, it seems still difficult to obtain the $\tau - Re$ relationship in a sufficiently wide Re range as for pipe flow. Nevertheless, given that a fully developed turbulent band resembles a turbulent puff in terms of the transient behaviour, as shown here, this memoryless transient characteristic is possibly retained at higher Re in channel flow also, i.e. turbulence becomes globally sustained by proliferation outweighing decay as in pipe flow.

On the other hand, the proliferation of a band is more complex and still poorly understood. It can be through longitudinal proliferation (i.e. nucleating a parallel daughter band at the tail, on the upstream side) or through transverse branching (nucleating a daughter band that takes the opposite orientation, on the downstream side) (Paranjape 2019; Shimizu & Manneville 2019; Mukund *et al.* 2021; Marensi *et al.* 2023). It was reported that the longitudinal proliferation process is band-length-dependent (Mukund *et al.* 2021), namely, the process is likely history-dependent rather than memoryless, unlike the splitting of a turbulent puff (Avila *et al.* 2011). Meanwhile, there still lacks a quantitative study for the transverse branching. Since history-independent proliferation is also an ingredient of DP, elucidating all these aspects is necessary for understanding the channel flow transition and clarifying its relationship with DP (Hof 2022).

Supplementary movies. Supplementary movies are available at https://doi.org/10.1017/jfm.2025.299.

Acknowledgement. The simulations were performed on Tianhe-1(A) at the National Supercomputer Centre in Tianjin.

Funding. The authors acknowledge financial support from the National Natural Science Foundation of China under grant numbers 12272264, 12322209 and 91852105. The work is also supported by The Fundamental Research Funds for the Central Universities, Peking University.

Declaration of interests. The authors declare no conflicting interests.

https://doi.org/10.1017/jfm.2025.299 Published online by Cambridge University Press

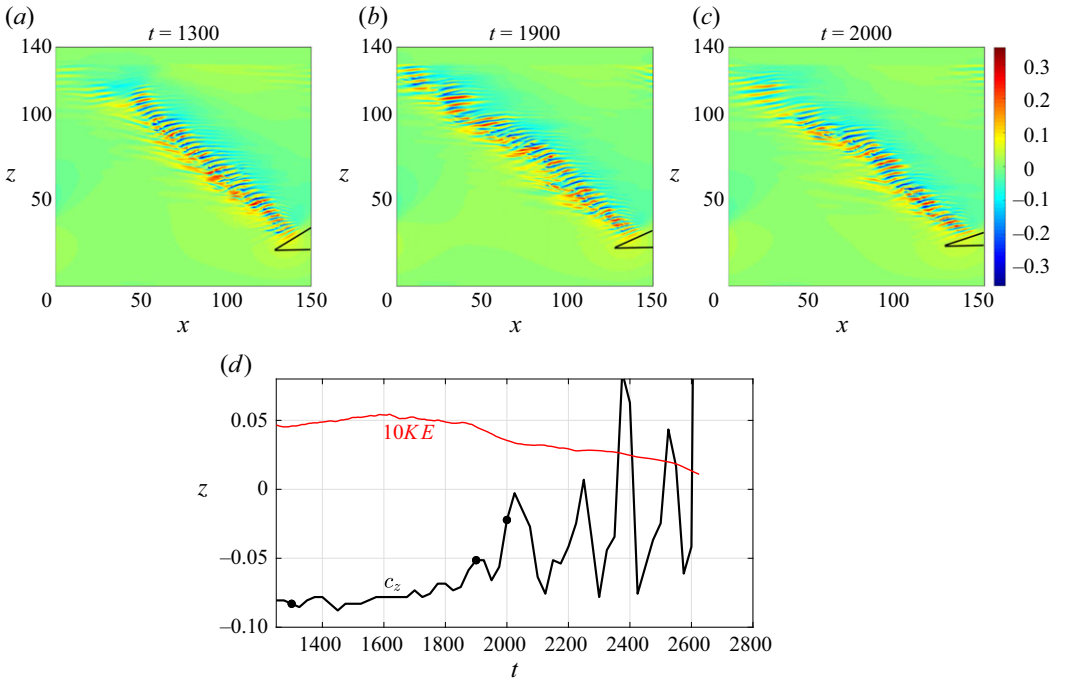


Figure 6. Illustration of the decay of a turbulent band. (*a–c*) Streamwise velocity perturbation u_x visualised in the cut-plane $y = -0.5$ at three time instants. The black angle at the head shows the tilt angle of the first high-speed streak (in colour red) about the streamwise direction. (*d*) The spanwise speed of the head c_z and the kinetic energy (scaled by a factor 10) of this run. The three black circles corresponds to time instances shown in (*a–c*).

Appendix A. Decay of a turbulent band

The decay process of a much shorter (i.e. much more constrained) turbulent band was reported by Xu & Song (2022), where it was shown that the whole band decayed coherently. Here we show that the decay of a much more extended turbulent band appears to be coherent also. Figure 6 shows the decay of a band at $Re = 640$ with the $L_z = 100$ damping setting. At $t = 1300$, when $c_z \approx -0.082$, the band has not started decaying. After $t = 1800$, the decay process started, signalled by the noticeably reduced tilt angle of the velocity streaks generated at the head and spontaneous decrease of the speed of the head (e.g. $c_z \approx -0.05$ at $t = 1900$) (see figure 6*b, d*). At $t = 2000$, the tilt angles of the streaks at the head had decreased further and so did c_z. The bulk part of the band does not show a significant change comparing $t = 1300$ and 1900, but the tail part at $t = 1900$ became more diffusive, showing reduced coherency, although the band was visually even slightly longer than it was at $t = 1300$. The total kinetic energy at $t = 1900$ was only slightly lower than that at $t = 1300$ although the decay had already started. At $t = 2000$, the tail part broke down further, showing a shrinking tendency from the two ends while the bulk part still looks rather similar to that of a non-decaying band.

Before the band completely decayed, one could observe strong oscillations in c_z. This may be attributed to attempts of the band to reform a turbulence-generating head. This can be seen from supplementary movie 2 after $t = 2000$. In all of our simulations, once the speed c_z drops below the threshold $|c_z| \approx 0.07$, the turbulent band never survived and the flow would relaminarise within approximately 1000 time units. A similar decay process of the turbulence in another run can be seen in supplementary movie 3.

https://doi.org/10.1017/jfm.2025.299 Published online by Cambridge University Press

The observation here indicates that the initialisation of the decay is neither due to a band breaking down into pieces nor due to continuous shrinking; instead, the whole band starts to decay as a coherent entity. It appears that the head undergoes a spontaneous decay first and then the whole band decays. Nevertheless, there should be a contribution from the bulk region to the decay of the head because our results showed an influence of the size of the band on the lifetime. So far, the understanding of the detailed mechanism is still poor and further studies are needed to elucidate this problem.

References

Avila, K., Moxey, D., De Lozar, A., Avila, M., Barkley, D. & Hof, B. 2011 The onset of turbulence in pipe flow. *Science* **333** (6039), 192–196.

Avila, M., Willis, A.P. & Hof, B. 2010 On the transient nature of localized pipe flow turbulence. *J. Fluid Mech.* **646**, 127–136.

Barkley, D. 2016 Theoretical perspective on the route to turbulence in a pipe. *J. Fluid Mech.* **803**, P1.

Borrero-Echeverry, D., Schatz, M.F. & Tagg, R. 2010 Transient turbulence in Taylor–Couette flow. *Phys. Rev. E* **81** (2), 025301.

Chantry, M., Tuckerman, L.S. & Barkley, D. 2017 Universal continuous transition to turbulence in a planar shear flow. *J. Fluid Mech.* **824**, R1.

Faisst, H. & Eckhardt, B. 2004 Sensitive dependence on initial conditions in transition to turbulence in pipe flow. *J. Fluid Mech.* **504**, 343–352.

Gomé, S., Tuckerman, L.S. & Barkley, D. 2020 Statistical transition to turbulence in plane channel flow. *Phys. Rev. Fluids* **5** (8), 083905.

Gomé, S., Tuckerman, L.S. & Barkley, D. 2022 Extreme events in transitional turbulence. *Trans. R. Soc. A* **380** (2226), 20210036.

Hinrichsen, H. 2000 Non-equilibrium critical phenomena and phase transitions into absorbing states. *Adv. Phys.* **49** (7), 815–958.

Hof, B. 2022 Directed percolation and the transition to turbulence. *Nat. Rev. Phys.* **5** (1), 62–72.

Hof, B., de Lozar, A., Kuik, D.J. & Westerweel, J. 2008 Repeller or attractor? selecting the dynamical model for the onset of turbulence in pipe flow. *Phys. Rev. Lett.* **101** (21), 214501.

Hof, B., Westerweel, J., Schneider, T.M. & Eckhardt, B. 2006 Finite lifetime of turbulence in shear flows. *Nature* **443** (7107), 59–62.

Kanazawa, T. 2018 Lifetime and growing process of localized turbulence in plane channel flow. PhD thesis, Osaka University, Japan.

Kashyap, P.V., Duguet, Y. & Dauchot, O. 2020 Flow statistics in the transitional regime of plane channel flow. *Entropy* **22** (9), 1001.

Klotz, L., Lemoult, G., Avila, K. & Hof, B. 2022 Phase transition to turbulence in spatially extended shear flows. *Phys. Rev. Lett.* **128** (1), 014502.

Lemoult, G., Mukund, V., Shih, H.-Y., Linga, G., Mathiesen, J., Goldenfeld, N. & Hof, B. 2024 Directed percolation and puff jamming near the transition to pipe turbulence. *Nat. Phys.* **20** (8), 1339–1345.

Lemoult, G., Shi, L., Avila, K., Jalikop, S.V., Avila, M. & Hof, B. 2016 Directed percolation phase transition to sustained turbulence in Couette flow. *Nat. Phys.* **12** (3), 254–258.

Marensi, E., Yalniz, G. & Hof, B. 2023 Dynamics and proliferation of turbulent stripes in plane-Poiseuille and plane-Couette flows. *J. Fluid Mech.* **974**, A21.

Mukund, V., Paranjape, C., Sitte, M.P. & Hof, B. 2021 Aging and memory of transitional turbulence. https://arxiv.org/abs/2112.06537.

Paranjape, C.S. 2019 Onset of turbulence in plane Poiseuille flow. PhD thesis, IST Austria.

Peixinho, J. & Mullin, T. 2006 Decay of turbulence in pipe flow. *Phys. Rev. Lett.* **96** (9), 094501.

Schneider, T.M. & Eckhardt, B. 2008 Lifetime statistics in transitional pipe flow. *Phys. Rev. E* **78** (4), 046310.

Shi, L., Avila, M. & Hof, B. 2013 Scale invariance at the onset of turbulence in Couette flow. *Phys. Rev. Lett.* **110** (20), 204502.

Shih, H.-Y., Hsieh, T.-L. & Goldenfeld, N. 2016 Ecological collapse and the emergence of travelling waves at the onset of shear turbulence. *Nat. Phys.* **12** (3), 245–248.

Shimizu, M. & Manneville, P. 2019 Bifurcations to turbulence in transitional channel flow. *Phys. Rev. Fluids* **4** (11), 113903.

https://doi.org/10.1017/jfm.2025.299 Published online by Cambridge University Press

SONG, B. & XIAO, X. 2020 Trigger turbulent bands directly at low Reynolds numbers in channel flow using a moving-force technique. *J. Fluid Mech.* **903**, A43.

TAO, J.J., ECKHARDT, B. & XIONG, X.M. 2018 Extended localized structures and the onset of turbulence in channel flow. *Phys. Rev. Fluids* **3** (1), 011902(R).

TSUKAHARA, T., SEKI, Y., KAWAMURA, H. & TOCHIO, D. 2005 DNS of turbulent channel flow at very low Reynolds numbers. In *Proceedings of the Fourth International Symposium on Turbulence and Shear Flow Phenomena, Williamsburg, VA, USA, 27-29 June*, pp. 935–940.

TUCKERMAN, L.S., KREILOS, T., SHROBSDORFF, H., SCHNEIDER, T.M. & GIBSON, J.F. 2014 Turbulent-laminar patterns in plane Poiseuille flow. *Phys. Fluids* **26** (11), 114103.

WILLIS, A.P. & KERSWELL, R.R. 2007 Critical behavior in the relaminarization of localized turbulence in pipe flow. *J. Fluid Mech.* **98** (1), 014501.

WU, H. & SONG, B. 2022 A numerical study of the side-wall effects on turbulent bands in channel flow at transitional Reynolds numbers. *Comput. Fluids* **240**, 105420.

XIAO, X. & SONG, B. 2020*a* The growth mechanism of turbulent bands in channel flow at low Reynolds numbers. *J. Fluid Mech.* **883**, R1.

XIAO, X. & SONG, B. 2020*b* Kinematics and dynamics of turbulent bands at low Reynolds numbers in channel flow. *Entropy* **22** (10), 1167.

XIONG, X.M., TAO, J., CHEN, S. & BRANDT, L. 2015 Turbulent bands in plane-Poiseuille flow at moderate Reynolds numbers. *Phys. Fluids* **27** (4), 041702.

XU, D. & SONG, B. 2022 Size-dependent transition nature of localized turbulence in transitional channel flow. *J. Fluid Mech.* **950**, R3.

ZHANG, L. & TAO, J. 2023 Large-scale mean flow and inclination of isolated turbulent band in channel flow. https://arxiv.org/abs/2310.03238.

https://doi.org/10.1017/jfm.2025.299 Published online by Cambridge University Press